Infrared imaging spectroscopy of Mars: H2O mapping and determination of CO2 isotopic ratios

Thérèse Encrenaz, Bruno Bézard, Tobias C. Owen, Sébastien Lebonnois, Franck Lefèvre, Thomas K. Greathouse, Matthew J. Richter, John H. Lacy, Sushil K. Atreya, Ah-San Wong, et al.

▶ **To cite this version:**

Thérèse Encrenaz, Bruno Bézard, Tobias C. Owen, Sébastien Lebonnois, Franck Lefèvre, et al.. Infrared imaging spectroscopy of Mars: H2O mapping and determination of CO2 isotopic ratios. Icarus, 2005, 179 (1), pp.43-54. ⟨10.1016/j.icarus.2005.06.022⟩. ⟨hal-03742575⟩

HAL Id: hal-03742575

https://hal.science/hal-03742575v1

Submitted on 28 Apr 2025

HAL is a multi-disciplinary open access archive for the deposit and dissemination of scientific research documents, whether they are published or not. The documents may come from teaching and research institutions in France or abroad, or from public or private research centers.

L'archive ouverte pluridisciplinaire **HAL**, est destinée au dépôt et à la diffusion de documents scientifiques de niveau recherche, publiés ou non, émanant des établissements d'enseignement et de recherche français ou étrangers, des laboratoires publics ou privés.

HAL Authorization

Infrared imaging spectroscopy of Mars: H_2O mapping and determination of CO_2 isotopic ratios

Th. Encrenaz [a,*,1], B. Bézard [a], T. Owen [b], S. Lebonnois [c], F. Lefèvre [d], T. Greathouse [e], M. Richter [f,1], J. Lacy [g,1], S. Atreya [h], A.S. Wong [h], F. Forget [c]

[a] *LESIA, CNRS-UMR 8109, Observatoire de Paris, F-92195 Meudon, France*
[b] *Institute for Astronomy, University of Hawaii, Honolulu, HI 92822, USA*
[c] *Laboratoire de Météorologie Dynamique, 5 place Jussieu, F-75231 Paris cedex 05, France*
[d] *Service d'Aéronomie, 5 place Jussieu, F-75231 Paris cedex 05, France*
[e] *Lunar and Planetary Institute, 3600 Bay Area Bvd., Houston, TX 77058-1113, USA*
[f] *Physics Department, University of California Davis, CA 95616, USA*
[g] *Department of Astronomy, University of Texas at Austin, RLM 15.308, C-1400 Austin, TX 78712-1083, USA*
[h] *Department of Atmospheric, Oceanic and Space Sciences, University of Michigan, Ann Arbor, MI 48109-2143, USA*

High-resolution infrared imaging spectroscopy of Mars has been achieved at the NASA Infrared Telescope Facility (IRTF) on June 19–21, 2003, using the Texas Echelon Cross Echelle Spectrograph (TEXES). The areocentric longitude was 206°. Following the detection and mapping of hydrogen peroxide H_2O_2 [Encrenaz et al., 2004. Icarus 170, 424–429], we have derived, using the same data set, a map of the water vapor abundance. The results appear in good overall agreement with the TES results and with the predictions of the Global Circulation Model (GCM) developed at the Laboratory of Dynamical Meteorology (LMD), with a maximum abundance of water vapor of $3 \pm 1.5 \times 10^{-4}$ (17 ± 9 pr-μm). We have searched for CH_4 over the martian disk, but were unable to detect it. Our upper limits are consistent with earlier reports on the methane abundance on Mars. Finally, we have obtained new measurements of CO_2 isotopic ratios in Mars. As compared to the terrestrial values, these values are: $(^{18}O/^{17}O)[M/E] = 1.03 \pm 0.09$; $(^{13}C/^{12}C)[M/E] = 1.00 \pm 0.11$. In conclusion, in contrast with the analysis of Krasnopolsky et al. [1996. Icarus 124, 553–568], we conclude that the derived martian isotopic ratios do not show evidence for a departure from their terrestrial values.

Keywords: Mars; Mars, atmosphere; Atmospheres, composition; Infrared observations

1. Introduction

The recent detections of martian H_2O_2 (Clancy et al., 2004; Encrenaz et al., 2004, hereafter called E04) and CH_4 (Krasnopolsky et al., 2004; Formisano et al., 2004; Mumma et al., 2003, 2004) have illustrated the capability of high-resolution spectroscopy in the infrared and submillimeter range to investigate the composition of the martian atmosphere. In particular, the use of current ground-based infrared imaging spectrometers allows us to map the martian disk at high spatial resolution (better than 1 arcsec) and spectral resolving power (10^4–10^5).

In June 2003, we have obtained infrared images of Mars around 8 μm at high spectral resolution, which have been used to detect and map hydrogen peroxide H_2O_2 on Mars

* Corresponding author. Fax: +33 1 45 07 28 06.
E-mail address: therese.encrenaz@obspm.fr (Th. Encrenaz).

[1] Visiting Astronomer at the Infrared Telescope Facility, which is operated by the University of Hawaii under Cooperative Agreement NCC 5-538 with the National Aeronautics and Space Administration, Office of Space Science, Planetary Astronomy Program.

Accepted Manuscript

(E04). This minor species, which had been unsuccessfully searched for over the past 25 years, is an important element of the martian photochemistry, which might be responsible for the absence of organics on the surface of Mars.

In the present paper, we show a new analysis of the same data set, which has led to a map of surface temperatures and a map of the spatial distribution of water vapor. The simultaneous mapping of H_2O and H_2O_2 can be directly compared to the predictions of the Global Circulation Model (GCM) developed at the Laboratory of Dynamical Meteorology (Forget et al., 1999; Lefèvre et al., 2004), under the same seasonal conditions. We have also used our data set to search for CH_4 variations over the martian disk, but no detection was achieved. Finally, we have obtained a new determination of the CO_2 isotopic ratios in Mars. These values, if different from the terrestrial ones, could provide important clues about the past history of the martian climate and/or possible non-thermal fractionation effects. Previous analyses of martian oxygen isotopes in H_2O (Bjoraker et al., 1989), and C and O isotopes in CO_2 (Krasnopolsky et al., 1996) have indicated a possible departure of the martian values from the terrestrial ones. As will be shown below, our determinations of C and O isotopic ratios in the martian CO_2 appear to be in agreement with the terrestrial values.

Our observations and modeling are described in Sections 2 and 3, respectively. Results on the surface temperature, the water mapping and the search for CH_4 are presented and discussed in Section 4. The analysis of the CO_2 isotopic ratios is presented in Section 5. Conclusions are summarized in Section 6.

2. Observations

Observations of Mars were carried out on June 19–21, 2003, using the Texas Echelon Cross Echelle Spectrograph (TEXES) mounted at the 3-m NASA Infrared Telescope Facility (IRTF) at Mauna Kea Observatory (Hawaii). This instrument can cover the 5–25 μm range with high spatial (0.3 arcsec pixel size) and spectral (7×10^4) resolution capabilities (Lacy et al., 2002). Two spectral intervals were covered during our run: 1230–1236 cm^{-1} (8.09–8.13 μm, June 19), and 1237–1244 cm^{-1} (8.04–8.08 μm, June 20). The spectral resolution was 0.016 cm^{-1}, corresponding to a resolving power of 7.7×10^4. These intervals were initially selected for the study of H_2O_2.

At the time of our observations, the diameter of Mars was 15 arcsec and the areocentric longitude was 206° (beginning of southern spring). Mars was approaching the Earth with a radial velocity of −11 km/s, corresponding to a Doppler shift of +0.045 cm^{-1}. The latitudes of the subsolar point (SSP) and the subterrestrial point (STP) were 11 S and 21 S, respectively. The local time of the STP was 15:00 and its western longitude ranged from 57° to 115°. The western longitude of the SSP covered the 97°–155° range. In June 2003, the dust opacity was minimal ($\tau = 0.2$ at 9 μm, MGS-TES Team, private communication).

For all data sets, our 1.1 × 8 arcsec slit was oriented along the celestial N–S axis, and the telescope was stepped by 0.5″ E between two successive 8-s integrations. The slit covered alternatively the northern and southern parts of the martian hemispheres in order to build two maps, for the northern and southern hemispheres, respectively. The pixel size was 0.3 arcsec. Our spatial resolution, after binning, was about 1.5 arcsec (E04). In the regions of strongest continuum, the S/N per spectrum is higher than 100, if the statistical noise only is considered. It is above 1000 in the averaged spectra corresponding to the subsolar area (see Figs. 1 and 2 of E04). Uncorrected telluric and instrumental fringing features are much larger than the statistical noise, but are broad compared to the martian lines.

The 1237–1244 cm^{-1} range (Fig. 1) shows the martian spectrum averaged over a region surrounding the subsolar point, where the S/N is found to be maximum (see E04). The spectrum exhibits, in addition to telluric features mostly due to CH_4 and H_2O, martian lines of H_2O_2, $^{13}C^{16}O^{17}O$ (637) and $^{13}C^{16}O^{18}O$ (638). The CO_2 isotopic lines have been used in the present study to retrieve the $^{18}O/^{17}O$ ratio in the martian CO_2. This spectral interval also exhibits strong terrestrial absorption lines due to H_2O, HDO, and CH_4. One martian absorption feature, due to H_2O, is detected in the wing of the corresponding water terrestrial line at 1240 cm^{-1}, and has been used to map the H_2O distribution on the martian disk. No martian CH_4 absorption was directly detected in the wings of the telluric methane lines; we searched for possible absorption fluctuations, over the martian disk, at the position of the expected Doppler-shifted transition, in order to obtain an upper limit of the CH_4 local

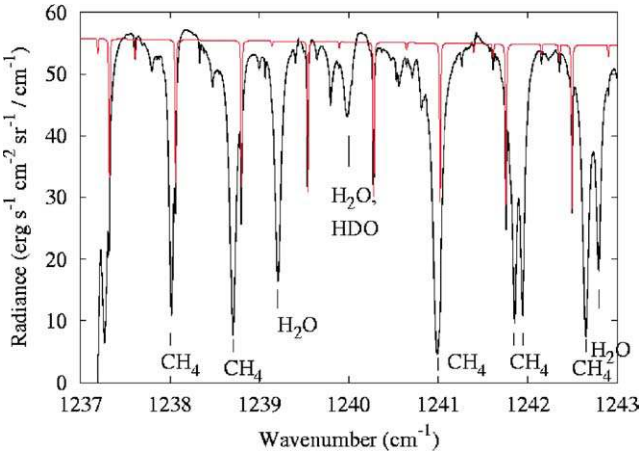

Fig. 1. A mean spectrum of Mars in the 1237–1244 cm^{-1} range, averaged in a region surrounding the subsolar point. A synthetic spectrum of the martian CO_2 is also shown, for the identification of the CO_2 isotopic lines. The spectrum is uncorrected for telluric absorption. The strongest absorption lines are due to terrestrial CH_4 and H_2O. The CO_2 synthetic spectrum is shifted by +0.045 cm^{-1} to account for the martian Doppler shift.

Accepted Manuscript

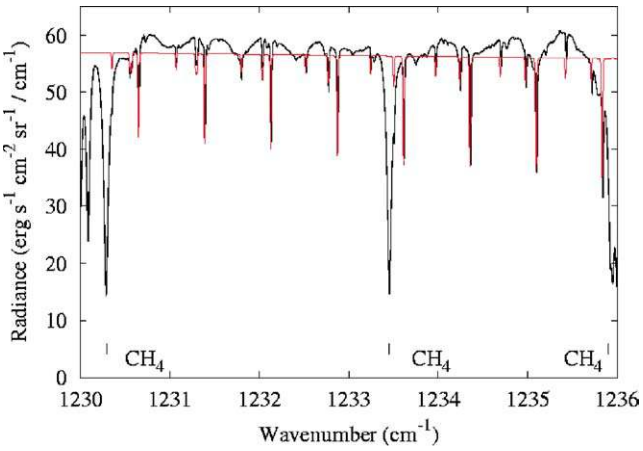

Fig. 2. A mean spectrum of Mars in the 1230–1236 cm^{-1} range, averaged in a region surrounding the subsolar point. A synthetic spectrum of the martian CO_2 is also shown, for the identification of the CO_2 isotopic lines. The spectrum is uncorrected for telluric absorption. The strongest absorption lines are due to terrestrial CH_4. The CO_2 synthetic spectrum is shifted by +0.045 cm^{-1} to account for the martian Doppler shift.

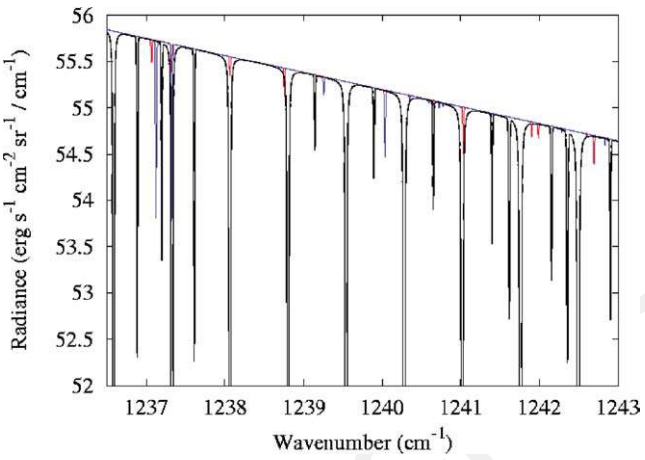

Fig. 3. A synthetic spectrum of Mars, calculated under nominal conditions (see text), including absorptions by CO_2 ($P_s = 5$ mbar, in green), H_2O (200 ppm, in blue) and CH_4 (100 ppb, in red).

variations on Mars. In addition, a map of the surface temperature has been retrieved from the continuum.

The 1230–1236 cm^{-1} range (Fig. 2), observed on June 19, shows the martian spectrum, averaged over the same region as for Fig. 1. It also shows lines of martian H_2O_2, $^{12}C^{16}O^{18}O$ (628) and $^{13}C^{16}O^{18}O$ (638), superimposed with telluric absorption features. The same spectral interval was also previously studied in February 2001 ($L_s = 112°$) and was used to infer a stringent upper limit of the H_2O_2 abundance at this time of the seasonal cycle (Encrenaz et al., 2002). In the present study, we have combined this data set with the new one to infer the $^{12}C/^{13}C$ ratio in the martian CO_2, using the CO_2 isotopic lines.

3. Radiative transfer modeling

We have calculated synthetic spectra of the martian atmosphere including CO_2, H_2O, and CH_4 (Fig. 3). Spectroscopic data were taken from the GEISA data bank (Jacquinet-Husson, 1999). In addition, spectroscopic parameters of weak CO_2 isotopic lines, not included in the GEISA list, were calculated using the compilation of Rothman (1986), based on the analysis of Toth (1985). In order to study the depths of the CO_2 isotopic lines, we had to mimic the mean conditions over the whole disk. For this purpose, following the predictions of the LMD GCM, we have used a mean surface pressure of 5 mbar, a mean surface temperature of 250 K; the mean an air mass factor was 1.4. We have used a mean atmospheric temperature of 220 K at $z = 0$ km and 180 K at $z = 20$ km. For the restricted area surrounding the subsolar point, as we did for our H_2O_2 study (see E04), we have used a surface temperature of 290 K and an airmass factor of 1.5. As shown in Figs. 1 and 2, this synthetic spectrum represents well the depths of the CO_2 lines in this region.

We have been able to identify all the absorption features, with depths as low as about 0.3%, present in the martian averaged spectra shown in Figs. 1 and 2. All martian lines belong to H_2O_2, isotopic CO_2 and (in one case) HDO. All other absorption features are identified as telluric absorptions.

4. Surface temperatures and minor constituents

4.1. Surface temperatures

Fig. 4a shows a map of the surface temperatures measured from the continuum radiance at 1240.15 cm^{-1}. This wavenumber was chosen as it corresponds to a spectral range where the radiance is maximum (see Fig. 1). Fig. 4b shows, for comparison, the prediction of the GCM for the corresponding observing conditions. It can be seen that the overall agreement is good. There are some differences, however. The maximum value of T_s is reached in the vicinity of the SSP (310 K for TEXES and 300 K for the GCM); the GCM map shows the T_s maximum close to the SSP, while the TEXES maximum is slightly shifted (by about 1 h) toward the evening. The TEXES data can also be compared with the TES data recorded in September 1999 for the same L_s value ($L_s = 195°$–$205°$), at $LT = 14{:}00$ (Smith, private communication). On the TEXES map, this local time corresponds to a longitude of 80–100 W. The TES data reach a maximum of 287 K at a latitude of 9 S, with values of 278 K and 250 K for latitudes of 40 S and 40 N, respectively. The corresponding TEXES and GCM values of T_s are respectively 305 and 290 K at 9 S, 300 and 290 K at 40 S, and 250 K for both data sets at 40 N. It can be see that for high values of T_s, the TEXES data set is slightly above the GCM predictions while the TES data set is slightly below.

There is another noticeable discrepancy between TEXES and the GCM, as well as TES, in the vicinity of the south pole. According to the GCM, the southern polar cap, at the

Accepted Manuscript

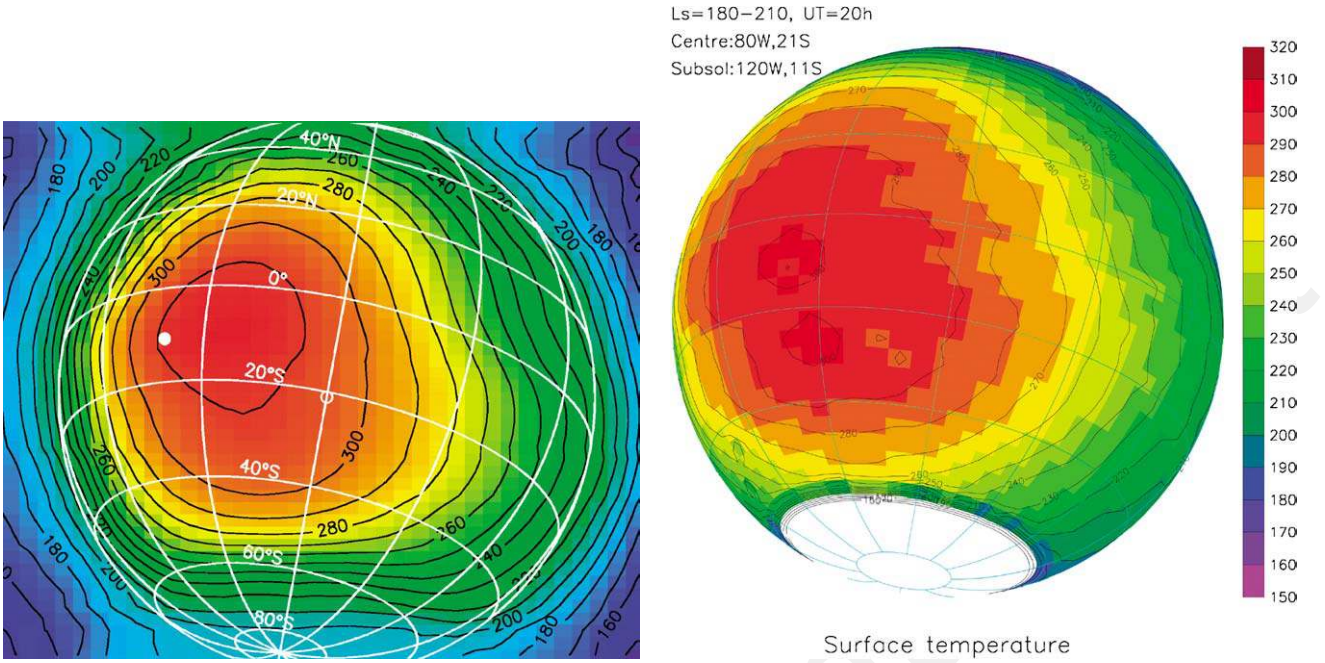

(a) (b)

Fig. 4. Surface temperatures of Mars retrieved from the TEXES data and compared with the GCM. (a) Surface temperatures measured with TEXES; the subsolar point is indicated with a white dot and the subterrestrial point with a circle. The mean longitude of the central meridian is 80 W and that of the subsolar point is 120 W. (b) Expected surface temperatures from the GCM, corresponding to the local and seasonal conditions of our observation.

beginning of southern spring ($L_s = 206°$), is expected to expand from the pole up to latitudes of $-60°$ S, and the surface temperature there should be lower than 150 K. This is confirmed by the TES measurements. In contrast, the surface brightness temperature measured by TEXES in this region ranges from 180 to 250 K. A plausible explanation could be that the spatial resolution in our data is not as high as the nominal value (1.5×1.5 arcsec). We note that the flux measured near the south pole is about one tenth of the maximum flux. This flux probably partly comes from the wings of the point spread function, which is close to a Lorentzian profile. Some smearing effect could also come from the uncertainty associated to image recentering.

It can be mentioned that the portion of Mars observed with TEXES (Fig. 4a) includes the Tharsis region, and that the highest surface temperatures (310 K) occur over a high-altitude region. Because the martian atmosphere is very thin, the situation is different from the Earth atmosphere where higher locations are usually cooler.

4.2. *Water vapor mapping*

Fig. 5a shows two observed spectra of Mars, averaged over the northern and southern hemisphere respectively, in the 1239.8–1240.7 cm^{-1} range. This spectral interval includes a telluric absorption line due to water at 1239.996 cm^{-1}, several CO_2 martian lines (in particular at 1240.25, 1240.53, and 1241.65 cm^{-1}) and a broader terrestrial absorption line at 1240.59 cm^{-1}. The water telluric absorption is actually the combination of two transitions; the ν_2 624 735 transition of HDO at 1239.995 cm^{-1}, with an energy level of 576.9 cm^{-1} and an intensity of 0.242×10^{-23} cm molec^{-1} (measured in the laboratory at room temperature), and the ν_2 827 854 transition of H_2O, with an energy level of 1255.2 cm^{-1} and an intensity of 0.702×10^{-23} cm molec^{-1}. In our modeling of the martian H_2O spectrum, we assume a martian D/H ratio of 5 times the terrestrial value (Krasnopolsky et al., 1997). As a result, the contribution of the HDO transition becomes predominant.

As illustrated by the strong CO_2 line at 1240.25 cm^{-1}, the martian absorption lines are deeper in the northern hemisphere than in the southern one, because, due to Mars' topography, the mean surface altitude is lower and the atmospheric path is thus longer. By dividing the northern spectrum by the southern spectrum (Fig. 5b), it is possible to separate the martian lines from the terrestrial absorptions, which should ideally completely disappear in the ratio. It can be seen that a CO_2 martian line indeed appears in absorption in Fig. 5b.

A weak line appears at 1240.04 cm^{-1}, in the blue wing of the terrestrial water line, in both north and south spectra (Fig. 5a). Its shift versus the central frequency of the terrestrial water line exactly corresponds to the Doppler shift of Mars, and we attribute this feature to martian water, as a combination of the HDO and H_2O transitions mentioned above (with HDO the major contributor). This identification is confirmed by the fact that the feature appears in absorption in Fig. 5b, as the other martian lines. Note that a weak martian H_2O_2 line is also present at the same frequency; however, its contribution is minor with regard to the HDO

Accepted Manuscript

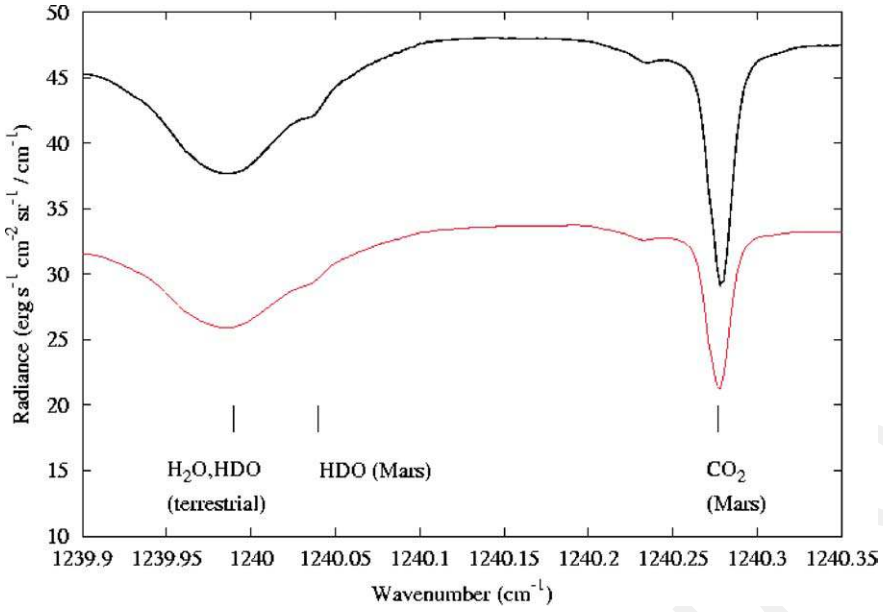

(a)

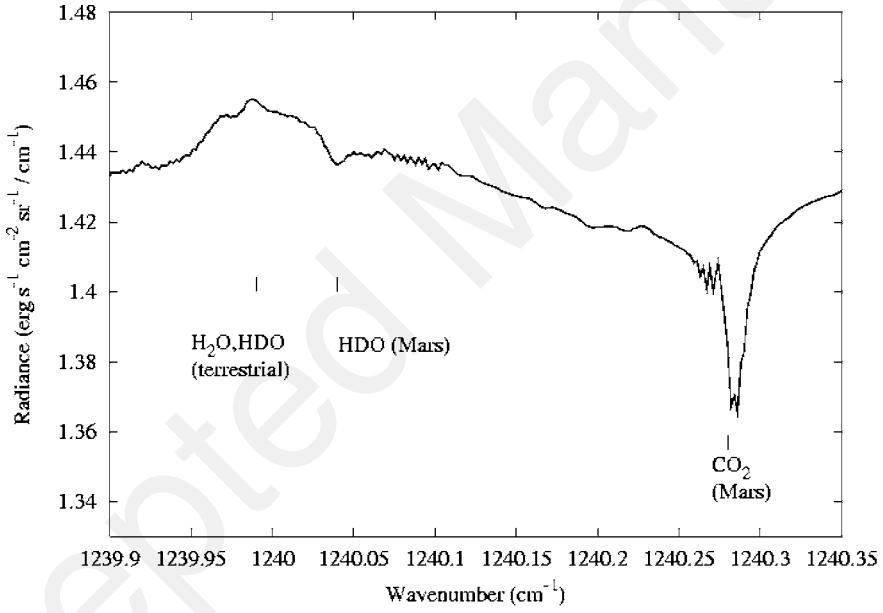

(b)

Fig. 5. (a) The TEXES spectrum in the 1239.9–1240.35 cm^{-1} range, averaged over the northern hemisphere (black) and the southern hemisphere (red). The broad absorption at 1240 cm^{-1} is terrestrial and due to H_2O + HDO. A weak absorption appears in the blue wing of this line. Its position corresponds to the Doppler shift due to the radial velocity of Mars, and is attributed to martian HDO. A martian CO_2 line also appears in the spectral range. (b) Ratio of the TEXES spectra in the northern and southern regions. The broad terrestrial absorption due to (H_2O, HDO) is removed in the ratio, and the martian lines still appear in absorption. In particular, the weak feature at 1240.04 cm^{-1} is shown in absorption, which shows that it is a martian line.

absorption. We have fitted the continuum on each side of the HDO martian line with a 2-order polynomial which fits well the observed spectrum. Fig. 6 shows the HDO line of the Mars subsolar spectrum (Fig. 5a), after removal of this continuum. The best fit is obtained for an H_2O surface mixing ratio of 3×10^{-4}, corresponding to a water column density of 17 pr-µm. Note that, under the conditions of our observation, water vapor saturation takes place at relatively high altitudes (about 30 km) so that, in our calculations, the H_2O mixing ratio and column density are almost proportional.

In order to map the water abundance over the martian disk, we have rationed the depth of the HDO martian line to a weak CO_2 line of comparable intensity, at 1241.6 cm^{-1}. This method was previously used, with the same CO_2 line, to map the H_2O_2 mixing ratio over the martian disk (E04). As discussed in this paper, this method minimizes the uncertainties due to effects of surface and atmospheric properties,

Accepted Manuscript

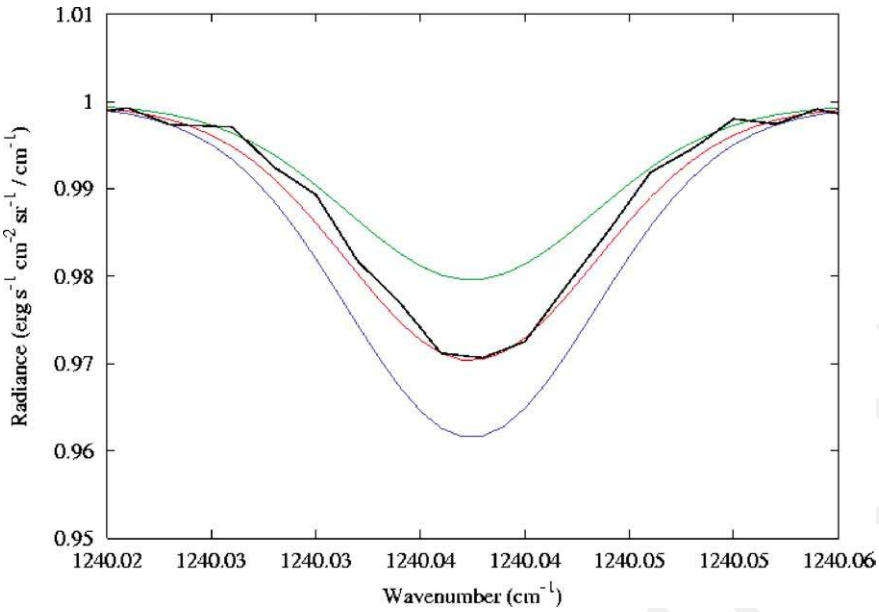

Fig. 6. The HDO martian line observed in the subsolar spectrum of Mars (same as Fig. 1), after removal of the continuum with a 2-order polynomial (black line), compared with synthetic spectra with different H_2O mixing ratios. Green: 200 ppm; red: 300 ppm; blue: 400 ppm. The D/H ratio in Mars is assumed to be 5 times the terrestrial value.

including topography, dust opacity and airmass factor. The map of the continuum is shown in Fig. 7a, and the maps of the CO_2 and HDO lines in Figs. 7b and 7c. The resulting H_2O map, derived from the HDO/CO_2 line depth ratio, is shown in Fig. 7d. It can be seen that the CO_2 and HDO line depths are maximum in the morning side near the equator. As noticed in E04, this results from the combination of two factors: (1) long atmospheric path (high airmass and low surface altitude (as this region corresponds to the south of Amazonis Planitia), and (2) a maximum contrast between the surface and atmospheric temperatures, due to a faster heating of the surface in the early morning. Fig. 7d shows the ratio of the HDO and CO_2 line depths; a line ratio of 0.5 corresponds to an H_2O mixing ratio of 3×10^{-4}.

The uncertainty on our H_2O result depends upon two factors: (1) the S/N of the TEXES data and (2) the uncertainty on the martian D/H ratio. The S/N of the North and South spectra (Fig. 5a) and the S/N of the subsolar spectrum (Fig. 1) are above 1000. The S/N on the HDO martian line depth is thus 15, while the one of the 1241.6 CO_2 line depth is 30. The corresponding H_2O mixing ratio for the subsolar spectrum is thus $3 \pm 0.3 \times 10^{-4}$, assuming a martian D/H ratio equal to 5 times the terrestrial value. However, the uncertainty on this determination is 40% (Krasnopolsky et al., 1997). Our H_2O determination thus becomes $3 \pm 1.5 \times 10^{-4}$ in the subsolar region. Because the uncertainty on the martian D/H is by far dominating the noise uncertainty, this error bar is valid over the whole region where the ratio is measured.

Fig. 8 shows the spatial distribution of H_2O calculated by the GCM for the martian geometric and seasonal conditions corresponding to our observation. It can be seen that the global distribution of H_2O is in good overall agreement with our results (Fig. 7d), both for the H_2O abundance and for its global distribution over the disk. The TEXES H_2O data indicate a slightly higher value, in particular near the SSP. There, the inferred H_2O mixing ratio is 3×10^{-4} while the GCM prediction is 2.2×10^{-4}. Taking into account our error bar, both results are consistent. Comparison with TES data (Smith, private communication) indicates a mean [H_2O] column density of about 20 pr-μm, also in agreement with our result. It can be recalled that the H_2O_2 maps inferred from the same data set shows a global general agreement with the GCM predictions, and a close agreement between the observed and predicted abundances (mixing ratio of 3×10^{-8}; E04).

Finally, we note that two other strong telluric water lines appear in the 1237–1244 cm^{-1} range, at 1239.219 cm^{-1} ($S = 0.593 \times 10^{-22}$ cm molec^{-1}) and 1242.799 cm^{-1} ($S = 0.336 \times 10^{-22}$ cm molec^{-1}), respectively. However, these lines have energy levels higher than 2000 cm^{-1}. As a result, these lines are expected to be weak in the martian atmosphere (see Fig. 3), and, in addition, they are very sensitive to the atmospheric temperature. Thus, these lines cannot be reliably used to map the martian water vapor.

4.3. Search for methane

In the 1237–1244 cm^{-1} range, three strong telluric absorption lines of methane can be considered for a search for martian methane in their blue wing, at a position shifted by 0.045 cm^{-1}. The three lines appear at 1238.712, 1240.995, and 1242.659 cm^{-1}. The second line, unfortunately, falls very close to a strong CO_2 line at 1241.979 cm^{-1} and has to be discarded for this reason.

Accepted Manuscript

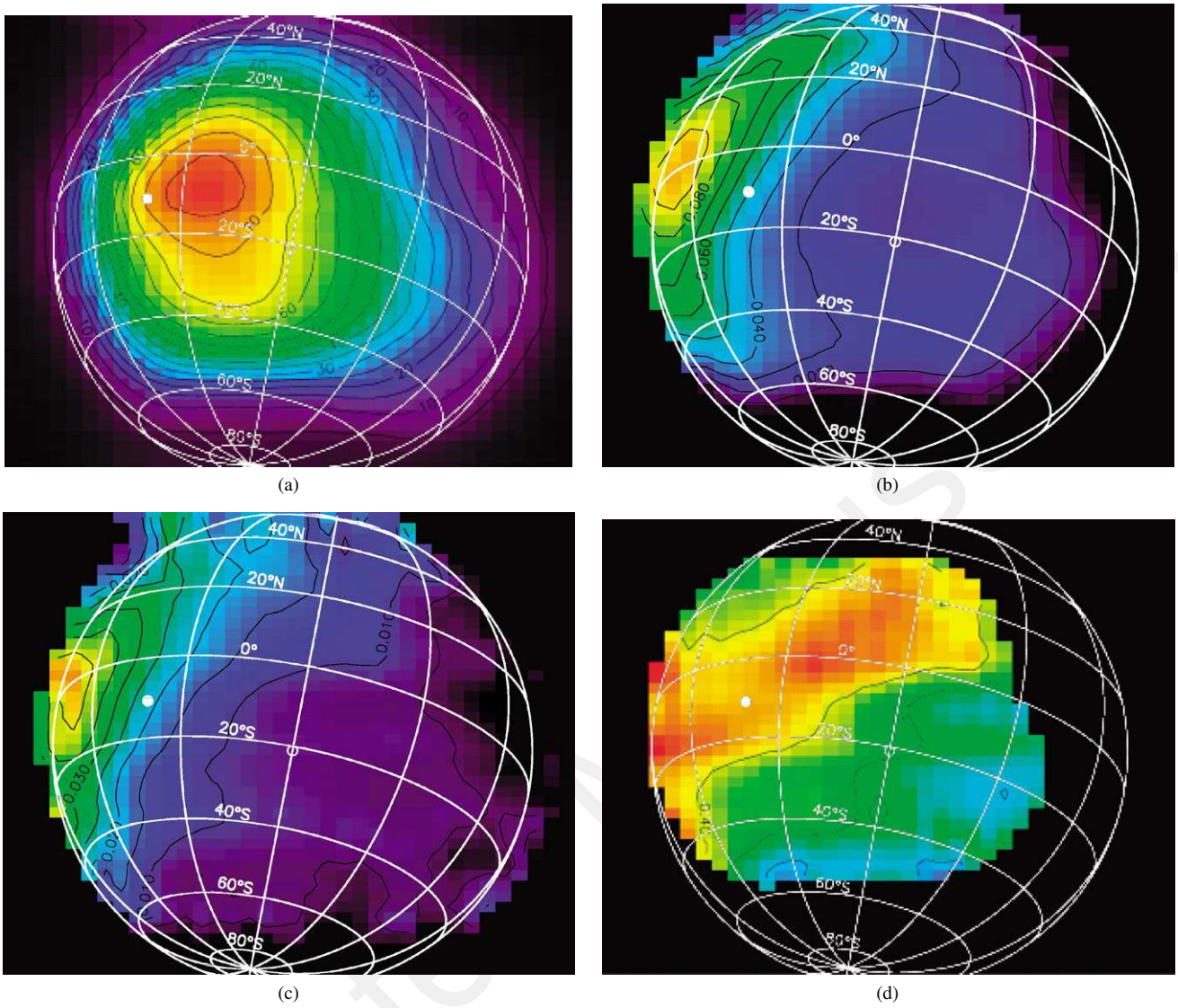

Fig. 7. Maps of (a) the continuum, (b) the CO_2 1241.6 cm^{-1} line depth, (c) the HDO 1240.04 cm^{-1} line depth, and (d) ratio of the HDO to CO_2 line depths. A line depth ratio of 0.5 corresponds to a H_2O mixing ratio of 3×10^{-4}. The subsolar point is indicated with a white dot and the subterrestrial point with a circle.

The 1242.659 cm^{-1} line is the (P_5, E_2 E_1) transition of the CH_4 ν_4 band, $S = 0.100 \times 10^{-19}$ cm molec^{-1}, $E =$ 575.18 cm^{-1}). Fig. 9 shows the averaged spectrum of Mars in the subsolar region (same as shown in Fig. 1), around the 1242.7 cm^{-1} CH_4 transition. The expected martian line, taking into account the Doppler shift, is at 1242.704 cm^{-1}. There is no evidence for CH_4 absorption, but the spectrum allows us to estimate the curvature of the spectrum, assuming the absence of methane absorption. At the center of the expected martian CH_4 line, the flux is 1.020 times the mean value linearly interpolated from the continuum on both sides, at ± 0.016 cm^{-1}. In order to search for possible methane variations over the disk, we have mapped the quantity

$$R = 1.020 - 2.0 \times I(1242.704) \Big/ \big[I(1242.688) + I(1242.720)\big],$$

where I is the observed TEXES intensity. Note that this measurement can provide information on methane variations only, but is somewhat uncertain for determining absolute methane abundances: it makes the assumption that the CH_4 column density is negligible in the subsolar region of Mars. The result is shown in Fig. 10. We consider that the signal enhancement in the southern region is likely to be meaningless, because it corresponds to a very weak continuum signal. Nevertheless, we note that a local maximum appears on the equator at the morning side, where the CO_2 line depth is also maximum (Fig. 7b). If real, the signal would correspond to a CH_4 line depth of 0.004, to be compared to the CO_2 line depth of 0.09. Comparing this ratio with the synthetic ratio for $CH_4 = 100$ ppb (0.143, see Fig. 3), we would infer, if the feature were significant, a CH_4 mixing ratio of 30 ppb. However, in view of the low level of the continuum at this position, the observed feature is probably a noise ef-

fect, as is probably also the case at other limb and southern positions. Indeed, a CH_4 line depth of 0.004 would require a continuum S/N on the order of 1000 to be significant, which occurs near the subsolar point but not at the limb.

Fig. 10 shows that there is no evidence for any variation of the methane absorption (with the exception of the western point mentioned above) in the whole latitude range $\pm 20°$, where the variations of the CH_4 line depth are below 0.002. Using again Figs. 3 and 7b, we infer that fluctuations of the methane mixing ratio are below 20 ppb on the morning side (where the CO_2 line depth is above 0.07) and below 70 ppb in the evening side (where the CO_2 line depth is above 0.02). Note again that, if the CH_4 mixing ratio was a few tens of ppb, uniformly distributed over the disk, our method would not be able to detect it (except possibly at the western point mentioned above).

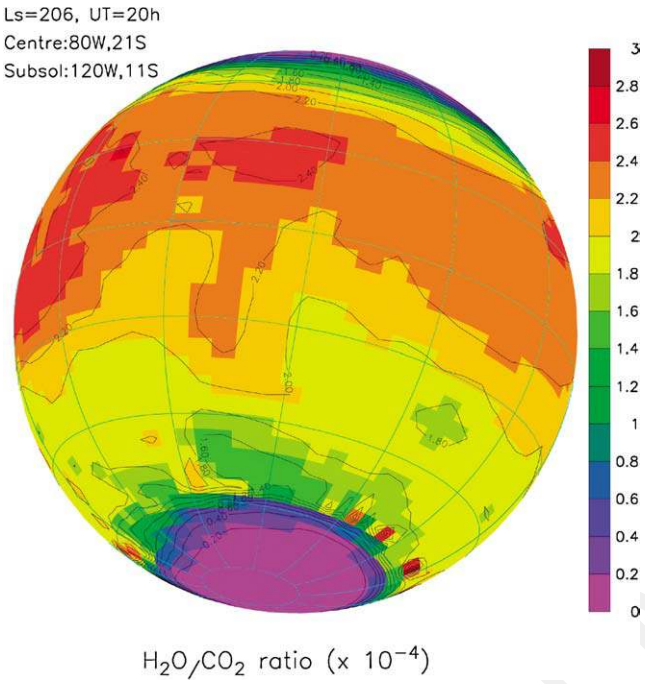

Fig. 8. Map of the H_2O mixing ratio, as modeled by the GCM under the conditions of our observations. This map is to be compared with Fig. 7d. The mean longitude of the central meridian is 80 W and that of the subsolar point is 120 W.

We have performed the same analysis on the 1238.712 cm^{-1} transition of methane ($P = 9$, $F_{2–6}$ $F_{1–2}$ of the ν_4 band; $S = 0.992 \times 10^{-20}$ cm molec^{-1}, $E = 575.26$ cm^{-1}), which is very similar to the first one, and we have obtained comparable results.

Our results do not contradict previous reported detections of methane on Mars. Following the first announcement of methane detection of CH_4 on Mars by Mumma et al. (2003), Krasnopolsky et al. (2004) using high-resolution ground-based spectroscopy at CFHT, reported the detection of methane with a mean mixing ratio of 10 ppb, which is below the detectability of the present study. Formisano et al. (2004) reported the detection of martian CH_4 using the PFS instrument aboard Mars Express, with a mean value of 10 ppb and local variations, from orbit to orbit, ranging from <5 to 35 ppb. More recently, Mumma et al. (2004) reported the detection of localized regions of enhanced methane abundance, at low latitudes, in particular at specific longitudes of 71° W (east of Valles Marineris) and −57° W (north of Hellas). Our upper limit on the evening side (70 ppb) does not contradict the first result. The second region is not observable in our field of view. Further measurements will be necessary, both from ground and space,

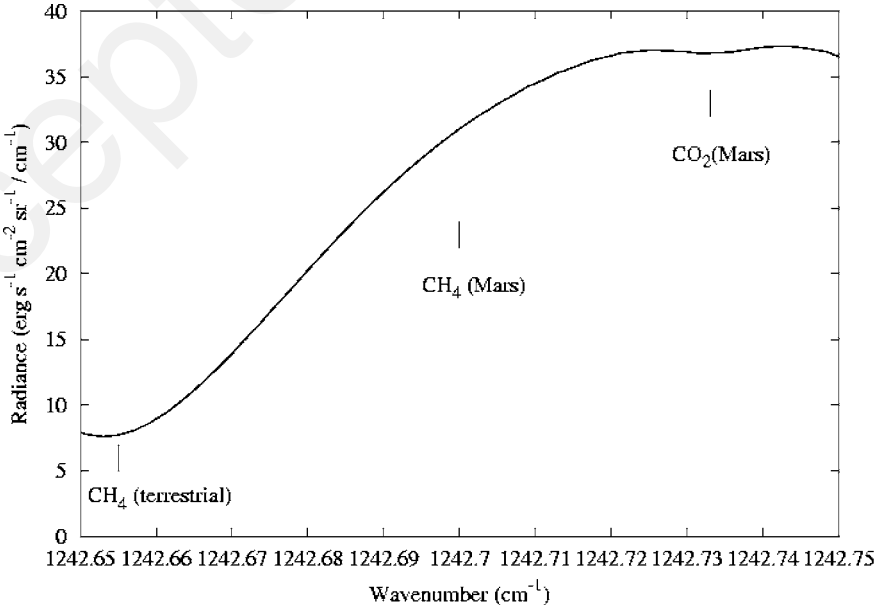

Fig. 9. The mean TEXES spectrum, averaged in a region surrounding the subsolar point (same as Fig. 1), around the frequency of the Doppler-shifted methane line 1242.7 cm^{-1}. Absorptions are due to the telluric methane line on the left, and to a weak martian CO_2 line on the right.

Accepted Manuscript

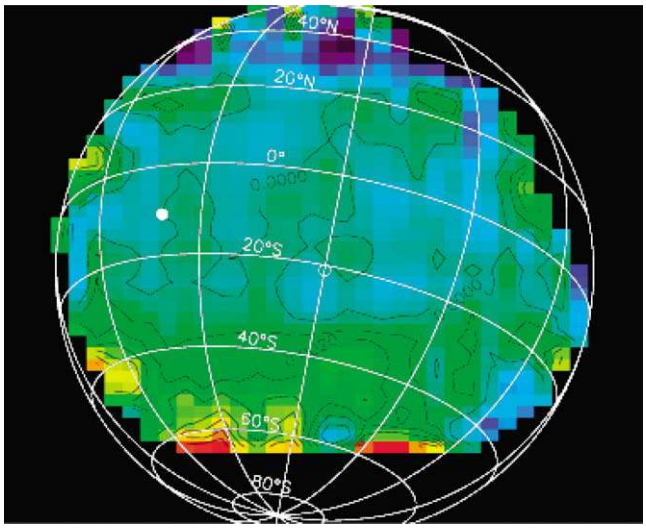

Fig. 10. Map of the R quantity, defined for the CH_4 1242.7 cm^{-1} line (see text). R is a possible indicator of the depth of the martian CH_4 line (if exists).

to confirm the methane detections previously reported in the near-infrared range.

5. Isotopic ratios in martian CO_2

A precise measurement of carbon and oxygen isotopes in the martian atmosphere can bring important clues about its history and evolution, and/or on non-thermal fractionation processes. In situ measurement by Viking reported, for carbon and oxygen, isotopic ratios in agreement with the terrestrial values within ±5% (Nier and McElroy, 1977), while the $^{15}N/^{14}N$ ratio was found to be enriched by a factor 1.6 (McElroy et al., 1977). The current interpretation was that Mars' primitive atmosphere would have been denser than now. A differential escape of nitrogen and hydrogen would have taken place over the planet's history, while the primordial CO_2 would have been trapped in the soil. This CO_2 reservoir would be able to exchange with the atmosphere, and keep the isotopic ratios equal to their terrestrial (and solar) values (Owen, 1992).

However, significant departures from terrestrial isotopic ratios were reported for oxygen in H_2O, and for both oxygen and carbon in CO_2. Using FTS spectra of the martian water vapor recorded with the Kuiper Airborne Observatory, Bjoraker et al. (1989) derived $^{17}O/^{16}O = 0.95 \pm 0.01$ and $^{18}O/^{16}O = 0.90 \pm 0.03$ relative to the terrestrial values. Using high-resolution ground-based spectra of Mars in the near-IR range, Krasnopolsky et al. (1996) measured, from martian CO_2 lines, $^{18}O/^{17}O = 0.914 \pm 0.04$ and $^{13}C/^{12}C = 0.94 \pm 0.15$ relative to the terrestrial values.

We have used the TEXES data to measure the $^{17}O/^{18}O$ and $^{13}C/^{12}C$ ratios in the martian CO_2, which allows a direct comparison with the latter results.

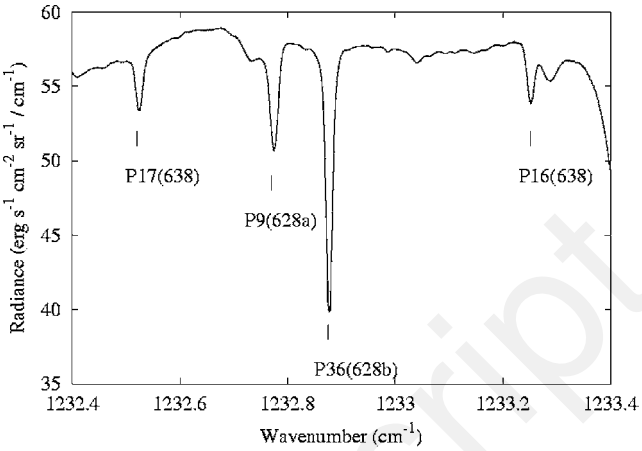

Fig. 11. The TEXES spectrum, averaged in an area surrounding the subsolar point (same as Fig. 1), in the 1232.4–1233.4 cm^{-1} spectral range. Several weak and strong CO_2 isotopic lines, belonging to the 627 and 628 bands, are present in this interval. The 627, 638, and 628-b lines belong to the (10002–00001) band; the 628-a line belongs to the (11102–01101) band.

5.1. Selection of isotopic lines and data sets

As shown in Figs. 1 and 2, several isotopic CO_2 bands of different intensities are present in the TEXES data. We have discarded the strongest (628) band (10002–00001) as the line depths are strongly dependent upon the thermal profile, and we have concentrated on the weak bands, which show typical line depths of a few percent at most (10002–00001 for the 627 and 638 bands, 11102–01101 for the 628 band). Synthetic modeling at full spectral resolution shows that these lines are not saturated. Measuring their line depths thus provides a direct measurement of the abundance of the isotopic species. We used the following method: we have compared, for a given isotopic species, the depths of the observed lines to the ones of a synthetic spectrum calculated with comparable atmospheric parameters, using terrestrial isotopic ratios. We have then averaged these ratios for each isotopic species and we have retrieved the martian isotopic ratios from the comparison of these ratios. A more complete description of the procedure is given below.

Fig. 11 shows a sample of the TEXES spectrum, averaged around the subsolar region, between 1232.4 and 1233.4 cm^{-1}, where several CO_2 isotopic lines are present. As mentioned above, the S/N in this spectrum is above 1000. It can be seen that the main uncertainty in the line depth measurement does not come from the statistical noise, but from the definition of the continuum level, which slightly varies over the martian surface. In order to reduce this uncertainty, we have divided our spectra in 3 subsets corresponding respectively to the northern hemisphere, the southern hemisphere and a small area where the continuum is maximum. We have performed our analyses on these 3 subsets independently, and we have averaged the results.

Accepted for Publication

Table 1
Isotopic line depths of 627 and 628 bands in the 1237–1244 cm^{-1} range

Band transition	Synthetic	Observed (north) Obs. N/synth.	Observed (south) Obs. S/synth.	Observed (max) Obs. M/synth.
627-P_{42}	0.0176	0.0179	0.0133	0.0151
		1.017	0.756	0.858
627-P_{41}	0.0254	0.0265	0.0195	0.0201
		1.043	0.768	0.791
627-P_{40}	0.0300	0.0290	0.0240	0.0270
		0.967	0.800	0.900
627-P_{39}	0.0354	0.0354	0.0260	0.0310
		1.000	0.734	0.856
Mean ratio-627 Obs./synth. ($\pm\sigma$)		1.007 ± 0.013	0.764 ± 0.012	0.829 ± 0.022
628-R_2	0.0393	0.0427	0.0313	0.0370
		1.086	0.796	0.941
628-R_3	0.0452	0.0437	0.0374	0.0342
		0.967	0.827	0.758
628-R_4	0.0418	0.0446	0.0330	0.0364
		1.069	0.789	0.871
Mean ratio-628 Obs./synth. ($\pm\sigma$)		1.041 ± 0.029	0.804 ± -0.009	0.857 ± 0.043
628/627 Obs./synth. ($\pm\sigma$)		1.034 ± 0.042	1.052 ± 0.021	1.001 ± 0.065

627 band: 10002–00001; 628 band: 11102–01101.

5.2. The $^{17}O/^{18}O$ ratio

In the 1237–1244 cm^{-1} range, we have selected 4 lines of the 627 band (P_{39} to P_{42}) and 3 lines of the 628 band (R_2 to R_4). Table 1 lists the synthetic and measured depths for the 3 subsets, and the inferred isotopic ratios. We note that in the case of the 628 band, the depth does not increase linearly with the J-number, because, as J increases, the line separates into a doublet which is resolved for $J > 3$.

5.3. The $^{13}C/^{12}C$ ratio

In the 1229–1236 cm^{-1} range, we have considered 7 lines from the 638 band (P_{13} to P_{19}) and 7 lines from the 628 band (P_5 to R_{12}). In addition to the 3 subsets mentioned above (north, south, maximum flux), we have also used a previous data set recorded in February 2001, which had been used to retrieve an upper limit of the H_2O_2 abundance (Encrenaz et al., 2002).

Table 2 lists the measured line depths in the 4 data sets, with the retrieved $^{13}C/^{12}C$ ratios.

6. Results and discussion

6.1. Instrumental uncertainty

Averaging the results listed at the bottom of Tables 1 and 2, and combining their error bars quadratically, we infer the following results:

$$\left[^{18}O/^{17}O\ (\text{Mars})\right]/\left[^{18}O/^{17}O\ (\text{Earth})\right] = 1.03 \pm 0.03,$$
$$\left[^{13}C/^{12}C\ (\text{Mars})\right]/\left[^{13}C/^{12}C\ (\text{Earth})\right] = 1.00 \pm 0.02.$$

We note, however, that estimating the error bars from the deviations of the individual lines may not be meaningful, especially for the $^{18}O/^{17}O$ ratio which relies on a small number of measurements (3 for the 628 band and 4 for the 627 band, respectively). This is illustrated by the fact that the differences between the measurements obtained from the different data subsets are larger than our error bars, which suggests that these error bars are underestimated. Thus, we have used an independent, more realistic way of estimating the uncertainty of our results. Because of the uncertainty on the definition of the continuum level, we estimate that the uncertainty in the depth measurement of a single line is 10%. Combining these uncertainties leads, for a given data subset, to an uncertainty of 0.05 for the 627 band and 0.07 for the 628 band, i.e., a total of 0.012 for the $^{18}O/^{17}O$ ratio. Co-adding the 3 data sets reduces this uncertainty to 0.07. In the case of the 638 and 628 band measurements, for which we use 7 lines in each case, the uncertainty for each band is 0.04, which leads to a total uncertainty of 0.08 for the $^{13}C/^{12}C$ ratio in each data subset. Co-adding the 4 data subsets leads to a final error of 0.04. Our results are thus:

$$\left[^{18}O/^{17}O\ (\text{Mars})\right]/\left[^{18}O/^{17}O\ (\text{Earth})\right] = 1.03 \pm 0.07,$$
$$\left[^{13}C/^{12}C\ (\text{Mars})\right]/\left[^{13}C/\ ^{12}C\ (\text{Earth})\right] = 1.00 \pm 0.04.$$

6.2. Uncertainty on the band intensities

We also have to consider the uncertainty associated with the spectroscopic measurement of the CO_2 bands we

Accepted Manuscript

Table 2
Isotopic line depths of 638 and 628 bands in the 1229–1236 cm^{-1} range

Band transition	Synthetic	Observed (N) Obs. N/synth.	Observed (S) Obs. S/synth.	Observed (max) Obs. M/synth.	Obs. Feb. 01 Obs. 01/synth.
638-P_{21}	0.047	–	–	–	0.050 1.066
638-P_{20}	0.050	–	–	–	0.050 1.000
638-P_{19}	0.053	0.048 0.906	0.043 0.811	0.041 0.773	0.054 1.021
638-P_{18}	0.055	0.052 0.945	0.046 0.836	0.038 0.691	0.055 0.991
638-P_{17}	0.058	0.045 0.776	0.041 0.707	0.042 0.724	0.059 1.024
638-P_{16}	0.060	0.046 0.767	0.042 0.700	0.042 0.700	0.059 0.983
638-P_{15}	0.061	0.048 0.787	0.043 0.705	0.043 0.705	
638-P_{14}	0.063	0.056 0.889	0.054 0.857	0.048 0.762	
638-P_{13}	0.063	0.049 0.778	0.048 0.762	0.043 0.683	
Mean rat. 638 Obs./synth. (σ)		0.835 ± 0.026	0.786 ± 0.023	0.720 ± 0.012	1.014 ± 0.011
628-P_{14}	0.062	–	–	–	0.061 0.998
628-P_{13}	0.061	–	–	–	0.059 0.959
628-P_{12}	0.061	0.043 0.705	0.042 0.688	0.045 0.738	0.059 0.967
628-P_{11}	0.064	0.055 0.859	0.049 0.766	0.050 0.781	0.064 1.000
628-P_{10}	0.080	0.065 0.812	0.060 0.750	0.056 0.700	–
628-P_9	0.087	0.078 0.897	0.074 0.851	0.065 0.747	0.088 1.011
628-P_8	0.095	–	–	–	0.082 0.858
628-P_7	0.090	0.074 0.822	0.063 0.700	0.064 0.711	0.079 0.881
628-P_6	0.077	0.070 0.909	0.063 0.818	0.064 0.831	–
628-P_5	0.067	0.059 0.874	0.058 0.859	0.053 0.791	–
Mean rat. 628 Obs./synth. (σ)		0.840 ± 0.024	0.776 ± 0.024	0.757 ± 0.016	0.953 ± 0.021
638/628 Obs./synth. (σ)		0.994 ± 0.050	1.013 ± 0.047	0.951 ± 0.028	1.064 ± 0.032

638 band: 10002–00001; 628 band: 11102–01101.

have used. According to Toth (1985), these uncertainties are 3% for the 628 band (11102–01101), 8% for the 638 band (10002–00001) and 2% for the 627 band (10002–00001). Consequently, the associated uncertainty is 5% for the $^{18}O/^{17}O$ ratio and 11% for the $^{13}C/^{12}C$ ratio. Our final results, including both sources of uncertainty, are thus:

$$\left[^{18}O/^{17}O\ (\text{Mars})\right]/\left[^{18}O/^{17}O\ (\text{Earth})\right] = 1.03 \pm 0.09,$$

$$\left[^{13}C/^{12}C\ (\text{Mars})\right]/\left[^{13}C/^{12}C\ (\text{Earth})\right] = 1.00 \pm 0.11.$$

Our determinations of carbon and oxygen ratios in the martian CO_2 are consistent with earlier in situ measurements by Viking (Nier and McElroy, 1977; Owen, 1992) and show no evidence for a departure from the terrestrial values. Our $^{18}O/^{17}O$ ratio is higher than the value inferred by Krasnopolsky et al. (1996) which implied a depletion of the heavier isotope with respect to the terrestrial values. Our results are consistent with current models of the martian atmospheric evolution, and do not require any escape nor fractionation mechanism.

Accepted Manuscript

7. Conclusions

The present study illustrates the capability of high-resolution imaging spectroscopy in the thermal infrared range for monitoring the composition and seasonal evolution of the martian atmosphere. The main results of this work can be summarized as follows:

- We have obtained a map of surface temperatures in good overall agreement with the TES data base and with the predictions of the GCM under similar seasonal and local conditions. We note however that the TEXES results are slightly above the GCM predictions, while the TES results are slightly lower.
- We have retrieved a map of H_2O which, taking into account our error bars, is also consistent with the TES results as well as with the GCM predictions. Our observations, which led to the first mapping of martian H_2O_2 (E04), thus provide for the first time simultaneous maps of H_2O and H_2O_2 on Mars. In the future, ground-based monitoring of these constituents, as a function of the martian cycle, will be a significant input for photochemical models.
- We have searched for possible variations of the CH_4 abundance on Mars, but we have failed to detect it. Our upper limits appear consistent with previous published or announced reports on methane on Mars. Further measurements will be needed to confirm the methane detections reported by Krasnopolsky et al. (2004), Formisano et al. (2004), and Mumma et al. (2004). In the future, yearly monitoring should be made to search for its spatial and (possibly) temporal variations.
- We have obtained new measurements of the $^{18}O/^{17}O$ and $^{13}C/^{12}C$ isotopic ratios in martian CO_2, which appear to agree with the terrestrial values. This result is consistent with our current understanding of the origin and evolution of the martian atmosphere (Owen, 1992). Our results do not confirm those of Krasnopolsky et al. (1996), which implied a depletion of the heavier isotopes. Here again, further measurements will be needed to improve its error bars.

Finally, we should mention that we have not been able to measure the $^{18}O/^{16}O$ ratio, because there was no line from a 626 band occurring in the spectral range that we have observed. The $^{18}O/^{16}O$ ratio in martian CO_2 is also a key parameter for understanding martian atmospheric processes and possible surface/atmosphere interactions. In the future, it will be possible to measure this ratio accurately with high-resolution spectroscopy in the 930–970 cm^{-1} range, where lines from 626 and 628 bands, can be found with comparable intensities.

Acknowledgments

We are grateful to M. Mumma for giving us access to his results prior to publication, and to M. Smith for giving us access to the TES data. Observations with TEXES were supported by NSF Grant AST-0205518. T.E. and B.B. acknowledge support from the Centre National de la Recherche Scientifique.

References

Bjoraker, G.L., Mumma, M.J., Larson, H.P., 1989. Isotopic abundance ratios for hydrogen and oxygen in the martian atmosphere. Bull. Am. Astron. Soc. 21, 991.

Clancy, R.T., Sandor, B.J., Moriarty-Schiven, G.H., 2004. A measurement of the 362 GHz absorption line of Mars atmospheric H_2O_2. Icarus 168, 116–121.

Encrenaz, Th., Greathouse, T.K., Bezard, B., Atreya, S.K., Wong, A.S., Richter, M.J., Lacy, J.H., 2002. A stringent upper limit of the H_2O_2 abundance in the martian atmosphere. Astron. Astrophys. 396, 1037–1044.

Encrenaz, T., Bézard, B., Greathouse, T.K., Richter, M.J., Lacy, J.H., Atreya, S.K., Wong, A.S., Lebonnois, S., Lefèvre, F., Forget, F., 2004. Hydrogen peroxide on Mars: Evidence for spatial and temporal variations. Icarus 170, 424–429.

Forget, F., Hourdin, F., Fournier, R., Hourdin, C., Talagrand, O., Collins, M., Lewis, S.R., Read, P., Huot, J.-P., 1999. Improved general circulation models of the martian atmosphere from the surface and above 80 km. J. Geophys. Res. 104, 24155–24176.

Formisano, V., Atreya, S., Encrenaz, T., Ignatiev, N., Giuranna, M., 2004. Detection of methane in the martian atmosphere. Science 306, 1756–1761.

Jacquinet-Husson, N., 47 colleagues, 1999. The 1997 spectroscopic GEISA databank. J. Quant. Spectrosc. Radiat. Trans. 62, 205–254.

Krasnopolsky, V.A., Mumma, M.J., Bjoraker, G.L., Jennings, D.E., 1996. Oxygen and carbon isotope ratios in martian carbon dioxide: Measurements and implications for atmospheric evolution. Icarus 124, 553–568.

Krasnopolsky, V.A., Bjoraker, G.L., Mumma, M.J., Jennings, D.E., 1997. High-resolution spectroscopy of Mars at 3.7 and 8 μm: A sensitive search for H_2O_2, H_2CO, HCl, and CH_4, and detection of HDO. J. Geophys. Res. 102, 6525–6534.

Krasnopolsky, V.A., Maillard, J.-P., Owen, T., 2004. Detection of methane in the martian atmosphere: Evidence for life? Icarus 172, 537–547.

Lacy, J.H., Richter, M.J., Greathouse, T.K., Jaffe, D.T., Zhu, Q., 2002. TEXES: A sensitive high-resolution grating spectrograph for the mid-infrared. Publ. Astron. Soc. Pacific 114, 153–168.

Lefèvre, F., Lebonnois, S., Montmessin, F., Forget, F., 2004. Three-dimensional modeling of ozone on Mars. J. Geophys. Res. 109 (E7), E07004, doi:10.1029/2003JD004027.

McElroy, M.B., Kong, T.Y., Yung, Y.L., 1977. Photochemistry and evolution of Mars' atmosphere: Implication for the evolution of volatiles. Planet. Space Sci. 24, 4379–4388.

Mumma, M.J., Novak, R.E., DiSanti, M.A., Bonev, B.P., 2003. A sensitive search for methane on Mars. Bull. Am. Astron. Soc. 35, 937.

Mumma, M.J., Novak, R.E., DiSanti, M.A., Bonev, B.P., Dello Russo, N., 2004. Detection and mapping of methane and water on Mars. Bull. Am. Astron. Soc. 36, 1127.

Nier, A.O., McElroy, B.M., 1977. Composition and structure of the martian atmosphere: Preliminary results from Viking 1. Science 194, 68–70.

Owen, T., 1992. The composition and early history of the atmosphere of Mars. In: Kieffer, H.H., Jakosky, B.M., Snyder, C.W., Matthews, M.J. (Eds.), Mars. Univ. of Arizona Press, Tucson, pp. 818–834.

Rothman, L.S., 1986. Infrared energy levels and intensities of carbon dioxide, Part 3. Appl. Opt. 25, 1795–1816.

Toth, R.A., 1985. Line positions and strengths of CO_2 in the 1200–1430 cm^{-1} region. Appl. Opt. 24, 261–271.

Accepted Manuscript